Organic matter affects phosphorus recovery during vivianite crystallization

Changyu Li and Yanqing Sheng IWA

ABSTRACT

Vivianite crystallization is a promising route for phosphorus (P) recovery from P-rich wastewater. However, organic matter (OM) in wastewater may influence vivianite formation. In this study, the effects of four representative OMs, glucose, bovine serum albumin (BSA), humic acid (HA) and sodium alginate (SA), on P recovery by vivianite were investigated. The results showed that P recovery efficiency was inhibited by HA and SA, declining by 3.7% and 12.1% under HA (100 mg/L) and SA (800 mg/L), respectively. BSA, HA and SA affected the aggregated form of vivianite crystals. Vivianite particle size decreased in the presence of HA and SA. Subsequent mechanistic exploration indicated that the complexation between the OM and Fe^{2+} was the main cause of P recovery efficiency reduction. The coprecipitation of HA and SA with vivianite could reduce the zeta potential on the crystal surface, resulting in a smaller particle size. The nucleation sites provided by BSA and SA could transfer vivianite from single plate-like agglomerate to multilayer plate-like agglomerate. This study provided a better understanding of P recovery by vivianite from OM-rich wastewater.

Key words | bovine serum albumin, humic acid, organic matter, phosphorus recovery, vivianite

HIGHLIGHTS

- Glucose, BSA, HA and SA affected vivianite crystallization from wastewater.
- OM might reduce P recovery rate by competition adsorption of Fe^{2+}.
- The morphology of vivianite crystals were different under SA and BSA.
- Negative correlation presented between OM and Fe/P ratios during crystallization.

GRAPHICAL ABSTRACT

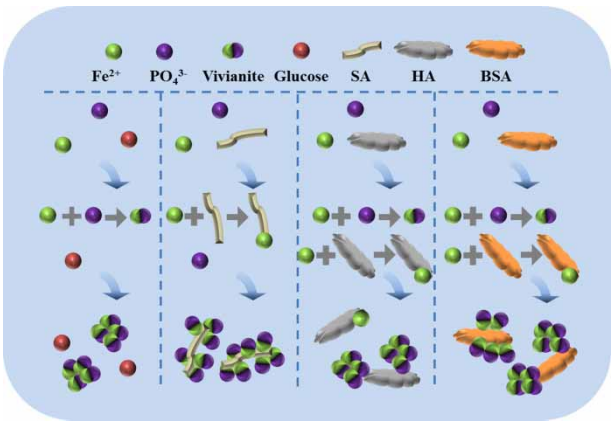

Changyu Li
Yanqing Sheng IWA (corresponding author)
Research Center for Coastal Environment Engineering Technology of Shandong Province,
Yantai Institute of Coastal Zone Research, Chinese Academy of Sciences,
Yantai,
China
E-mail: *yqsheng@yic.ac.cn*

Changyu Li
University of Chinese Academy of Sciences,
Beijing,
China

doi: 10.2166/wst.2021.112

INTRODUCTION

Phosphorous (P) is an indispensable biogenic element for living matter and plays a vital role in both biogenic growth and modern industry (Venkiteshwaran *et al.* 2018). Rock phosphate is a limited and nonrenewable resource that might be exhausted in several decades (Cordell *et al.* 2009; Hao *et al.* 2013). Therefore, a consensus has been reached regarding the serious shortage of P resources (Chowdhury *et al.* 2017). However, approximately 1.3 million tons of P are discharged into the environment with wastewater every year (Li & Li 2017). High P emissions have caused increasing crises in aquatic environments, especially for eutrophication (Huang *et al.* 2015; Park *et al.* 2017). If this wasted P is recovered, it can meet ~20% of global P demand (Yuan *et al.* 2012).

A promising strategy for P recovery (P_R) is the production of recyclable compounds, such as calcium phosphates, struvite and vivianite (Desmidt *et al.* 2015; Shaddel *et al.* 2019; Wu *et al.* 2019). In particular, vivianite [$Fe_3(PO_4)_2{\cdot}8H_2O$] crystallization has shown good application prospects due to its natural ubiquity, easy accessibility, and foreseeable economic value (Wu *et al.* 2019). Currently, many studies have confirmed the feasibility of applying vivianite crystallization to P_R from sludge (Cheng *et al.* 2015; Wilfert *et al.* 2016, 2018; Wang *et al.* 2019). In our previous study, it has been proven that it is possible to release P from the sludge phase into the liquid phase through excess sludge pretreatment followed by reprecipitation to obtain vivianite (Li & Sheng 2020). However, during the P release process, some organic substances and ionic impurities in sludge will be released simultaneously, which may affect vivianite crystallization (Wang *et al.* 2016; Madsen 2019).

There has been some attempts to delineate the key factors influencing vivianite formation, such as pH, the Fe/P molar ratio, the saturation index (*SI*) and coexisting metal ions (Liu *et al.* 2018; Wang *et al.* 2018). However, the effects of organic matter (OM) interference on vivianite precipitation are scarcely reported (Lin *et al.* 2020; Zhang *et al.* 2020). Generally, OM comprises abundant functional groups, e.g., carbonyls, carboxyls, hydroxyls, and ester groups, which may influence the properties of vivianite and the transformation of Fe^{2+} and orthophosphate (PO_4^{3-}-P) (He *et al.* 2014; Chen *et al.* 2019). Based on these studies, the effect of OM on the crystallization of calcium phosphates and struvite can be explained by: (1) the adsorption of OM on the crystallite surface and blockage of the active growth sites and (2) the complexation of organic ligands with metal ions in the solution and reduction of the free ions available for precipitation (Zhou *et al.* 2015). However, notably, the aforementioned studies treated OM as a whole and summarized the effect mechanism. OM in wastewater consists of a variety of large and small molecules. The concentration range, molecular weight (MW) distribution, and dominant functional groups are different for different molecular species. These factors make it difficult to explore the interference mechanism of different OM species. Therefore, using representative compounds might be a viable simulation to understand the interaction between OM and vivianite formation.

Collectively, organic compounds in sludge usually include saccharides (monosaccharides and polysaccharides), proteins and humic substances (Yuan *et al.* 2019). The polysaccharide released from granular sludge has similar properties to alginate (Lin *et al.* 2013). Glucose is a common monosaccharide, and the protein and humic substances in synthesizing artificial sewage are usually prepared with bovine serum albumin (BSA) and humic acid (HA) (Yang *et al.* 2012; Wei *et al.* 2019). Therefore, glucose, BSA, HA and sodium alginate (SA) could be used as representative OM to identify the effects on vivianite crystallization.

The objectives of this study were to investigate the effects of OM (glucose, BSA, HA, SA) on vivianite crystallization at different concentrations. After the precipitates were recovered, their composition, morphology and other characteristics were analyzed to explore the effects and their mechanisms. The results obtained in this study may provide new insights for P_R as vivianite from OM-rich wastewater.

MATERIALS AND METHODS

Preparation of synthetic wastewater

All the inorganic chemicals, glucose and SA used in the experiment were analytical reagent grade and purchased from Sinopharm Chemical Reagent Co., Ltd. HA and BSA (Biotech Grade) were purchased from Shanghai Aladdin Bio-Chem Technology Co., Ltd. Ferrous coagulant of $FeSO_4{\cdot}7H_2O$, which is commonly used in wastewater treatment plants (WTTPs), was selected as the Fe^{2+} source, and KH_2PO_4 was selected as the PO_4^{3-}-P source.

The PO_4^{3-}-P content in the sludge anaerobic digester of WTTPs can range from 75–400 mg/L (Garcia *et al.* 2012). Therefore, the content of PO_4^{3-}-P in this study was set at 310 mg/L (0.01 M). Typically, after sludge digestion, different OM concentrations in the wastewater were within the range of tens to thousands of mg/L. According to previous studies, the maximum carbohydrate, protein and HA concentrations can reach 800, 938.33 and 100 mg/L, respectively (Chen *et al.* 2007; Wei *et al.* 2019; Zhang *et al.* 2020). Therefore, the concentrations of glucose, HA, BSA and SA in synthetic wastewater ranged from 0–1,000 mg/L, 0–100 mg/L, 0–1,000 mg/L, and 0–800 mg/L, respectively. Oxygen-free deionized water was used in the experiments, and all the experiments were conducted in an anaerobic glove box with N_2 flushing at 25 °C. A stock solution of 0.2 M PO_4^{3-}-P was prepared from KH_2PO_4, and a stock solution of 0.3 M Fe^{2+} was prepared from $FeSO_4{\cdot}7H_2O$. The concentrations of glucose, SA, BSA and HA stock solutions were 20.0, 10.0, 20.0 and 5.0 g/L, respectively. Then, 50 mL PO_4^{3-}-P stock solution, 50 mL Fe^{2+} stock solution, and different amounts of OM stock solution were transferred into a 1000 mL volumetric flask for dilution with water and used as synthetic wastewater. The Fe/P molar ratio was 1.5 in the synthetic wastewater samples (Liu *et al.* 2018).

Crystallization experiments

Prepared synthetic wastewater was transferred to a 1,000 mL beaker and adjusted to pH 7.0 using 2 M NaOH and 2 M H_2SO_4 under magnetic stirring for 30 min before settling for 30 min. Then, the sample was centrifuged at 4,000 rpm for 10 min. The supernatants were used to measure PO_4^{3-}-P, Fe^{2+} and OM concentrations, and the separated solids were dried at 40 °C and ground for further analyses.

Mechanism analysis experiment

Premixing experiments were used to investigate the combination of different OM with Fe^{2+} or PO_4^{3-} separately. Fifty milliliters of Fe^{2+} stock solution (0.3 M) or PO_4^{3-}-P stock solution (0.2 M) were mixed with different amounts of OM stock solution and then transferred to a 1,000 mL volumetric flask for dilution with deionized water. The concentration of OM was similar to that in the vivianite experiments. The mixed solution pH was adjusted to 7.0 under magnetic stirring for 30 min before settling for 30 min (Liu *et al.* 2018). The concentrations of dissolved Fe^{2+} and PO_4^{3-}-P before and after the reaction were measured.

^{31}P nuclear magnetic resonance analyses (^{31}P-NMR) were used to validate the complexes between phosphorus and different OM. OM consisting of 100 mg glucose, 10 mg HA, 100 mg BSA, and 80 mg SA was mixed with 100 mL KH_2PO_4 solution (0.01 M) individually, and then the mixture was stirred for 2 h at pH 7.0. Then, it was centrifuged, filtered and concentrated to 10 mL at 40 °C for ^{31}P NMR analysis.

To determine the adsorption capacity of vivianite to OM, 0.1 g of pure vivianite was placed in 100 mL centrifuge tubes. Then, 50 mL of solution containing different OM was added (along with 0.01 M NaCl to maintain ionic strength). The gradient concentrations of OM were 0–100 mg/L. The solution pH was adjusted to 7.0 ± 0.2 using 0.1 M NaOH and 0.1 M HCl. The mixture was stirred at 200 rpm for 48 h until adsorption equilibrium was reached. At the end of the adsorption experiments, the OM concentration in the supernatants was determined.

The initial Fe/P molar ratios of 1.6–2.0 in synthetic wastewater were chosen to evaluate the effect of Fe/P on vivianite precipitation in the presence of OM. The synthetic wastewater was consistent with the abovementioned methods, and the OM concentrations were 1,000 mg/L glucose, 1,000 mg/L BSA, 100 mg/L HA and 800 mg/L SA. Moreover, the MW distribution of different OM was investigated. Details of the procedures are provided in Figure S1 (Supplementary material).

Analysis and calculation methods

A digital pH meter (PE28-Standard, Mettler) with a combined electrode (LE438) was used to determine the pH values. PO_4^{3-}-P and Fe^{2+} were determined following standard methods (APHA 2005). Anthrone-sulfuric acid colorimetry was used to determine glucose. BSA was determined by the Coomassie brilliant blue method. SA and HA were determined using a total organic carbon–nitrogen analyzer (TOC, VCPH, Shimadzu, Japan). For zeta potential measurement, 200 mg vivianite precipitates were dispersed in 100 mL phosphate buffer saline (0.05 M, pH 7.0) by ultrasound for 15 min. The zeta potential of the precipitate surface was measured by a potential analyzer (Zetasizer Nano ZS90, Malvern, UK). The particle size of the precipitates was measured by a laser particle analyzer (2000F, Malvern, UK). The micromorphology of the precipitates was analyzed using a high-resolution field emission scanning electron microscope (SEM, S-4800, Hitachi, Japan). The mineralogical composition was identified by powder X-ray diffraction analysis (XRD-7000, Shimadzu, Japan)

with Cu-K radiation (40 kV, 30 mA) in the 2θ range 10°–80°. The functional groups of the precipitates were analyzed by a Fourier transform infrared (FTIR) spectrometer (Nicolet iS10, Thermo Fisher, USA) with a capacity range 4,000–400 cm^{-1}. ^{31}P-NMR analysis was performed using a 500 MHz spectrometer (Advance III Bruker, Germany). D_2O was used for the field frequency lock prior to the experiment. All ^{31}P chemical shifts are relative to 85% orthophosphoric acid at 0 ppm.

The efficiency of the P_R was calculated using Equation (1):

$$P_R = \frac{P_0 - P_t}{P_0} \times 100\% \quad (1)$$

where P_0 (mg/L) and P_t (mg/L) are the PO_4^{3-} concentrations before and after precipitation, respectively.

The removal efficiency of the OM (O_R) was calculated using Equation (2):

$$O_R = \frac{R_0 - R_t}{R_0} \times 100\% \quad (2)$$

where R_0 (mg/L) and R_t (mg/L) are the OM concentrations in the supernatant before and after precipitation, respectively.

To understand the adsorption capacity of vivianite to OM, adsorption experiment data were fitted to the Langmuir adsorption model, which was given by the following:

$$q_e = \frac{kQ_mC_e}{1 + kC_e} \quad (3)$$

where q_e (mg/g) is the equilibrium adsorption capacity; k is the Langmuir constant, Q_m (mg/g) is the maximum adsorption capability, and C_e (mg/L) is the equilibrium concentration.

The *SI* level was defined by Equation (4):

$$SI = \lg \frac{\{Fe^{2+}\}^3\{PO_4^{3-}\}^2}{K_{SP}} \quad (4)$$

where K_{SP} represents the solubility constant of vivianite at 25 °C, fixed at $10^{-39.8}$ (Liu *et al.* 2018), and $\{Fe^{2+}\}$ and $\{PO_4^{3-}\}$ represent the ionic activity of Fe^{2+} and PO_4^{3-}, respectively; these values was calculated by Visual MINTEQ 3.0.

Data analysis

All tests were conducted in duplicate or triplicate. Analysis of variance was used to evaluate the significance of the results, and $p < 0.05$ was considered to be statistically significant. Data in this study are presented as the mean ± standard deviation.

RESULTS AND DISCUSSION

Effect of different OM on P recovery efficiency

The effect of OM gradients on P_R efficiency is shown in Figure 1. P_R reached 99.6% after reaction without added OM. With glucose added, the minimum P_R (98.3%) was observed at 600 mg/L, which represented only a 1.3% decrease compared with the control (without OM). This indicated that glucose had almost no effect on P_R. The effect of BSA was similar to that of glucose, and P_R did not decrease noticeably at different BSA concentration. The maximum residual PO_4^{3-}-P was 6.3 mg/L, suggesting that 98.0% of P participated after vivianite crystallization. HA inhibition for P_R was stronger than that of BSA. Compared with the control, the residual PO_4^{3-}-P increased from 1.40 to 12.45 mg/L with 100 mg/L HA. Moreover, SA inhibition on P_R was not observed at low concentrations, while P_R rapidly decreased to 87.7% as SA increased to 800 mg/L. Previous studies have shown that HA and SA had a strong adsorption capacity for divalent metal ions, which could account for the decline in P_R in this work (Park & Yoon 2009; Liu *et al.* 2012). This assumption was supported by the premixing experiments.

In the premixing experiments of OM with Fe^{2+}, the reduction of Fe^{2+} concentration is shown in Figure 1(c) and 1(d). After glucose and BSA were added to the $FeSO_4$ solution, the soluble Fe^{2+} was only reduced by 4 and 8 mg/L, respectively. A weak combining capacity was apparent between Fe^{2+} and glucose/BSA. Fe^{2+} reduction increased linearly with increasing HA concentration. At low SA concentrations, the reduction of Fe^{2+} concentration was not obvious, but it had a sharp increase at high SA concentrations. The Fe^{2+} concentration decreased by 36.5 and 60.8 mg/L at 100 mg/L HA and 800 mg/L SA, respectively. In contrast, the interaction of OM with PO_4^{3-} was not obvious, and the PO_4^{3-}-P concentration remained stable after OM addition (Figure S2). The ^{31}P NMR spectra of KH_2PO_4 solution with different OM were investigated separately (Figure S2). Specifically, the single signal of ^{31}P NMR

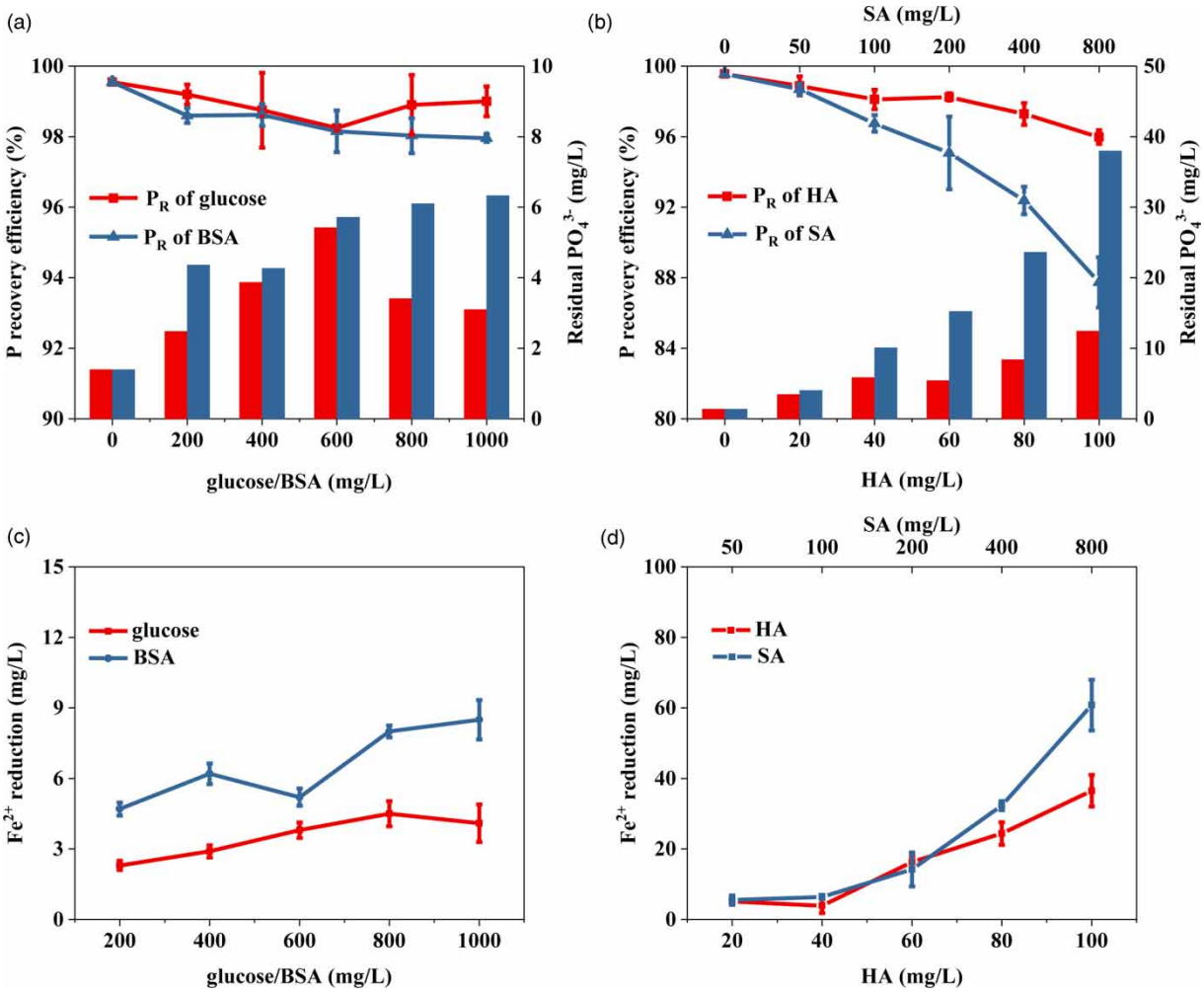

Figure 1 | (a) Effect of glucose and BSA on P recovery efficiency. (b). Effect of HA and SA on P recovery efficiency. (c) Fe^{2+} combination with glucose and BSA. (d) Fe^{2+} combination with HA and SA.

with different OM was observed at 0 ± 0.2 ppm without peak shifting, which was indicative of the weak binding ability between OM and PO_4^{3-}. Both OM solutions and PO_4^{3-} are electronegative, which may be the reason for the weak binding of OM and PO_4^{3-}. To conclude, it was confirmed that by competitive binding of Fe^{2+}, the presence of SA and HA resulted in adverse effects on P_R. The OM inhibition of P_R was in the following order: SA > HA > BSA > glucose.

Transfer of OM

During vivianite crystallization, OM might transfer to the solid phase through adsorption or coprecipitation with crystals, which would affect the purity of the harvested products. The residue of OM in the supernatant and the removal efficiency (O_R) variation are illustrated in Figure 2. At different glucose concentrations, the O_R values were less than 10.0%, indicating that most of the glucose remained in the liquid phase after vivianite crystallization. This result indicated that nearly no glucose reacted with Fe^{2+} and PO_4^{3-}, and glucose was not involved in the precipitates. However, for BSA and HA, O_R remained above 85% for all concentration gradients. These results showed that most of the BSA or HA in the liquid phase was transferred to the solid phase during the reaction. When the SA concentration was below 200 mg/L, most SA was fixed by precipitates, and the O_R reached 83.6%. However, ~30.0% SA remained in the supernatant with an SA concentration of 800 mg/L. The remaining SA could not be transferred to precipitates by centrifugation or filtrated through a 0.45 μm membrane. The synthetic wastewater after crystallization remained viscous.

The transfer of OM to the solid phase includes two pathways, coagulation by Fe^{2+} and coprecipitation after adsorption on the vivianite surface. In vivianite adsorption

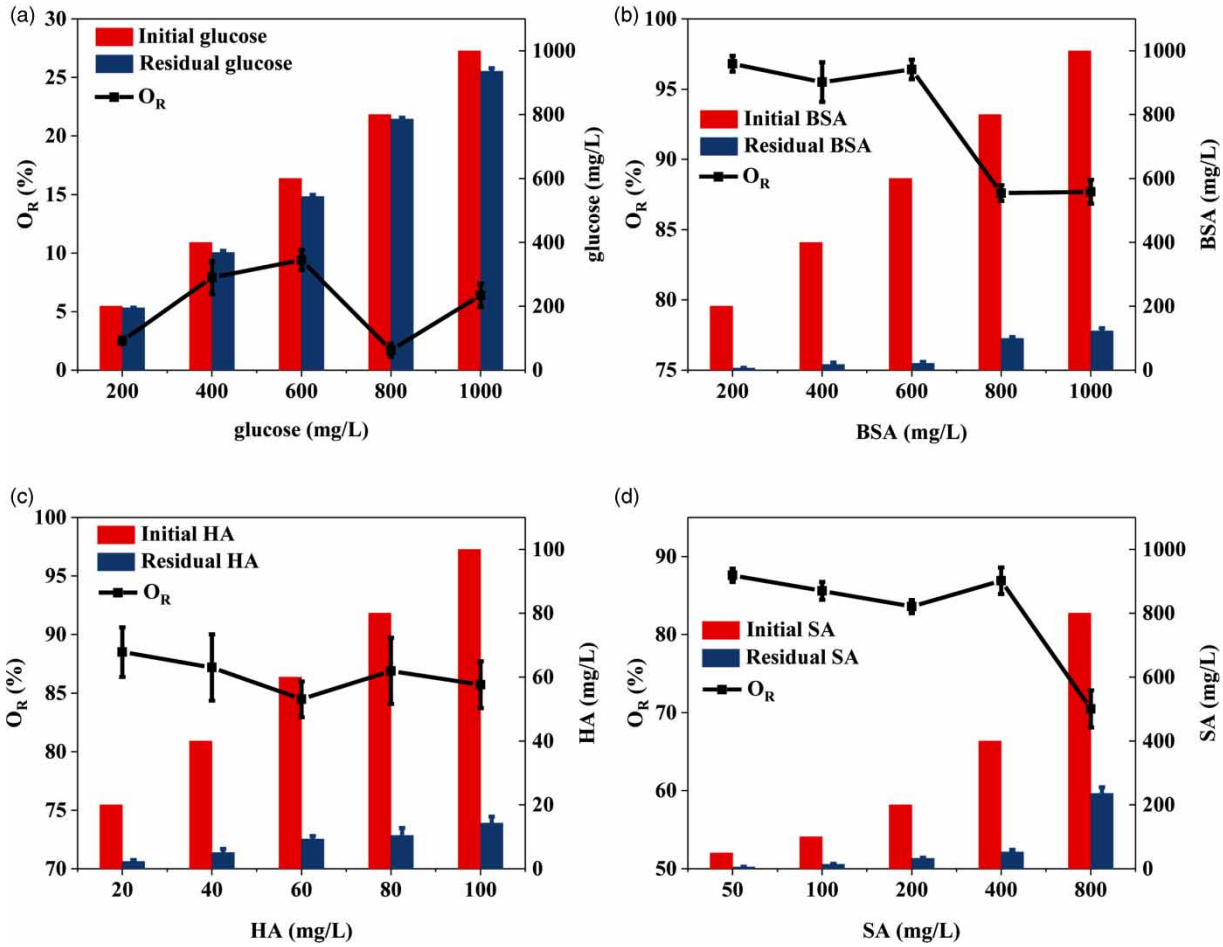

Figure 2 | The residue of OM and their removal efficiency: (a) glucose, (b) BSA, (c) HA and (d) SA.

experiments, the calculated maximum adsorption capabilities of glucose, BSA, HA and SA were 3.22, 7.69, 5.07 and 16.80 mg/g, respectively, which were far below the OM concentration reduction (Table S1, Supplementary material). BSA, HA and SA solution properties are similar to those of colloids. Charge neutralization of Fe^{2+} could destabilize the colloid, which might be the main cause of OM transfer to the solid. OM precipitation with vivianite would inhibit the crystal process and then the P_R. According to Figure 1, the P_R changing with HA and SA bore this out. Interestingly, however, BSA coprecipitation had little effect on P_R, which needs further explanation.

Effect of OM on recovered precipitates

The XRD patterns of precipitates with different OM are shown in Figure 3. Without OM addition, the recovered vivianite crystals showed strong and sharp diffraction peaks at 11.05°, 13.05°, 18.05°, 23.14°, 27.85°, 30.06° and 33.02° corresponding to Miller indices (110), (020), (200), (−201), (−131), (201) and (041), respectively. The result was consistent with the standard spectra of vivianite crystals (PDF#79-1928), indicating that the product was vivianite (Li *et al.* 2020). After addition of different OM, no significant difference was observed in the positions of the obtained precipitate peaks. This proved that the type of recovered product was not changed by the addition of OM. However, the presence of BSA and SA changed the relative intensity of the crystal diffraction peaks (Figure 3). The lattice plane relative strength of vivianite crystals (020) and (201) decreased by degrees with increasing BSA. This result suggested that BSA could alter the morphology of vivianite crystals. When the SA concentration ranged from 50 to 200 mg/L, the XRD patterns of the precipitates corresponded to the vivianite pattern. In comparison, when the SA concentration was increased to 800 mg/L, the intensity

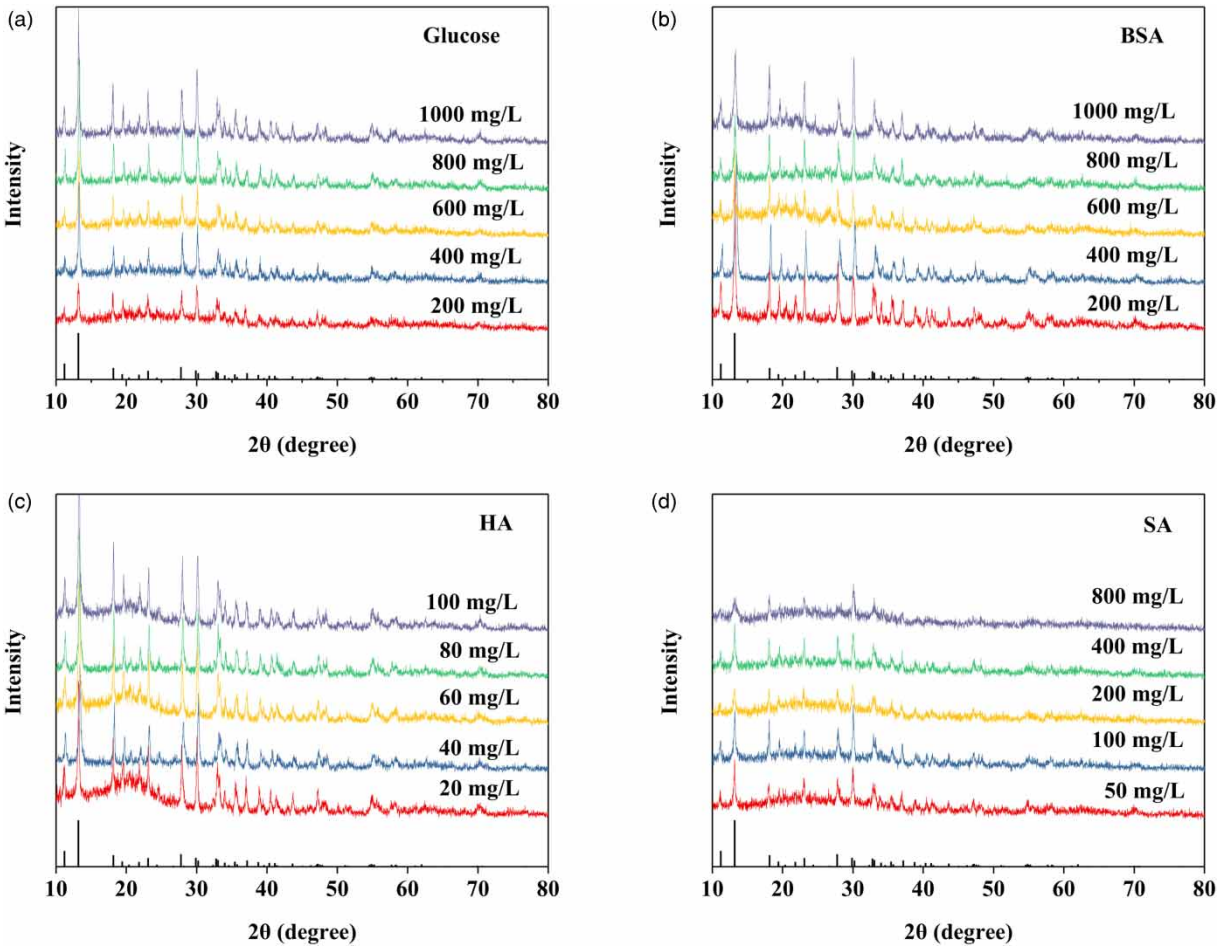

Figure 3 | XRD spectra of recovery products at different OM: (a) glucose, (b) BSA, (c) HA and (d) SA.

of the peak at 13.05° decreased significantly, and the increasing strength of the characteristic peaks at 30.06° showed that the crystals presented long dimensions in the (201) direction (Zhang *et al.* 2020).

Usually, crystallization can be divided into homogeneous and heterogeneous crystallization, which is related to the *SI*. When the *SI* was in the metastable zone, heterogeneous crystallization occurred, that is there was a growth of small crystals. When the *SI* was above the metastable zone, homogeneous crystallization occurred, namely, small crystal aggregation (Wang *et al.* 2014). A previous study has shown that the suitable supersaturation level for efficient vivianite crystallization could be in *SI* 4–11 (Liu *et al.* 2018). In this study, the initial *SI* was 15.1, so the aggregation of small crystals was dominant during crystallization. This result was further confirmed by SEM images of vivianite crystals with different OM (Figure 4 and Figure S3). In the absence of OM, the harvested crystal was an agglomerate of a single plate with a roughly spherical morphology. Zelibor *et al.* (1988) reported that vivianite occurs as spherical aggregates of platy-, lath- and needle-shaped crystals in different environments. However, in this study, with the presence of different OM, only plate crystals were observed. Although the surface of any individual crystal in the aggregates appeared to be randomly oriented, the crystals showed a definite crystal orientation, as if they generally radiated from a common center. Moreover, there were some amorphous substances on the crystal surface, and it was presumed to be adsorbed OM or Fe-P precipitation. The crystal transformed from a single plate-like agglomerates to a multilayer plate-like agglomerates with increasing BSA concentration (Figure 4). In contrast, with the addition of 800 mg/L SA, the products formed multiple layers of cumulative compounds rather than crystals with clear boundaries. Such changes in morphology were consistent with the XRD results. A likely explanation was that BSA and SA could penetrate into the interior of crystals and play a bonding role in the aggregate process.

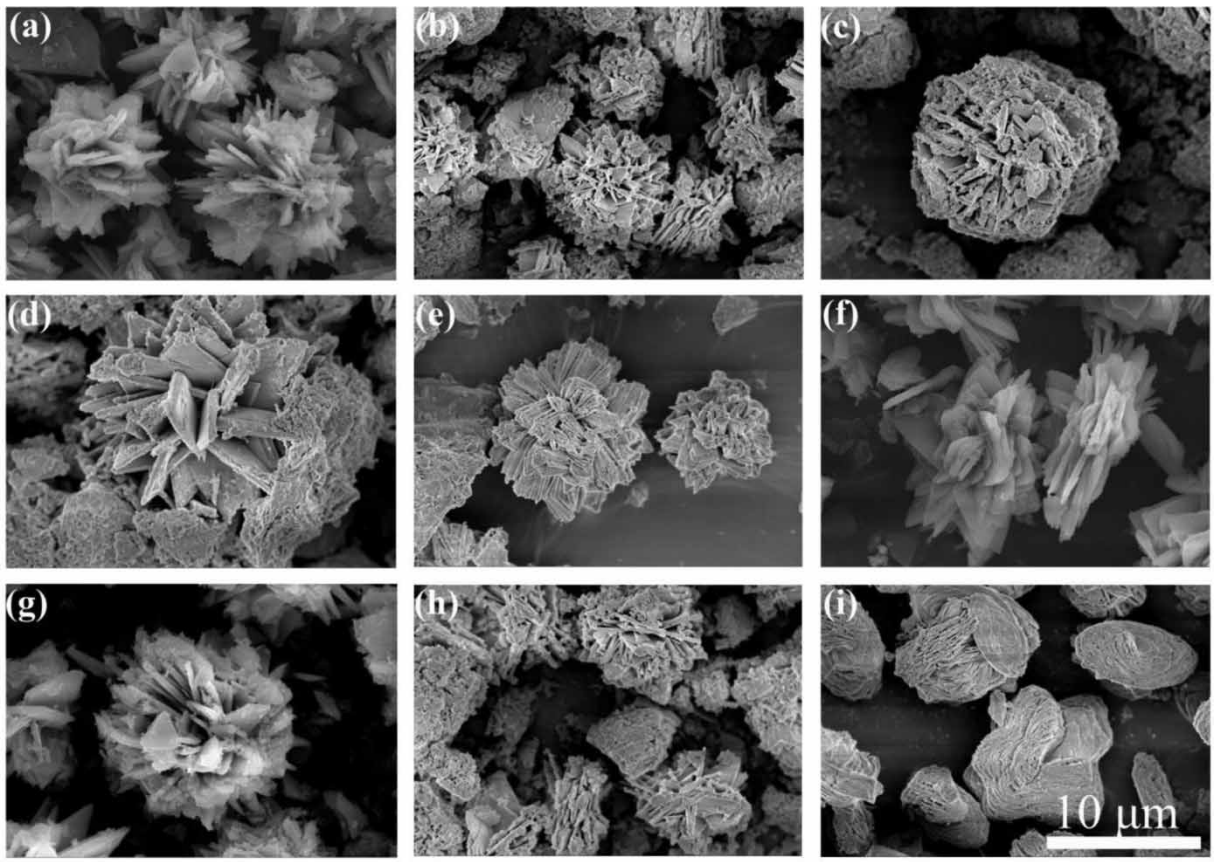

Figure 4 | SEM images of recovery products at different OM: (a) control; (b) 200 mg/L glucose; (c) 1,000 mg/L glucose; (d) 200 mg/L BSA; (e) 1,000 mg/L BSA; (f) 20 mg/L HA; (g) 100 mg/L HA; (h) 50 mg/L SA; (i) 800 mg/L SA.

The particle size changes of the products after OM addition are shown in Figure 5. The particle sizes of the precipitates presented two centralization distributions: one-micron and ten-micron scales. These bimodal distributions were consistent with the aggregative growth theory (Wang *et al.* 2014); small particles were formed in solution with supersaturation as the driving force, and large particles were formed by continued growth or direct fusion of small crystals. There was no significant effect on the particle size of the product from glucose addition. BSA addition could result in a 10-micron scale increase for the particle size, while a 1-micron scale increase was observed for HA addition. These results indicated that HA inhibited the further growth of small crystals. For SA (<800 mg/L), the product particle size was uniformly distributed from one to tens of microns, while it decreased significantly for concentrations over 800 mg/L (Figure 5). This result suggested that the increased solution viscosity might reduce the aggregation of small particles.

Figure 5 also illustrates the zeta potential variation of vivianite with different OM. It was noteworthy that larger vivianite particles had settled before zeta potential measuring. Therefore, the zeta potential reflects the surface potential of the remaining small particles (10 microns and below). Generally, a higher zeta potential (absolute value) on the particle surface results in less particle bonding. The dispersion system of agglomeration was more stable (Zhang *et al.* 2020). Compared with HA and SA, the effect of glucose and BSA addition on crystal surface potential changes was not significant. The zeta potential of the control was −15.5 mV, and it fluctuated with increasing concentrations of glucose and BSA. The minimum zeta potentials were −25.3 and −21.4 mV, respectively. After HA and SA addition, the zeta potential of the products was reduced to −44.2 and −56.1 mV, respectively. Lower zeta potential on the surface of the products inhibited the aggregative growth of small crystals and thus affected the distribution of particle size.

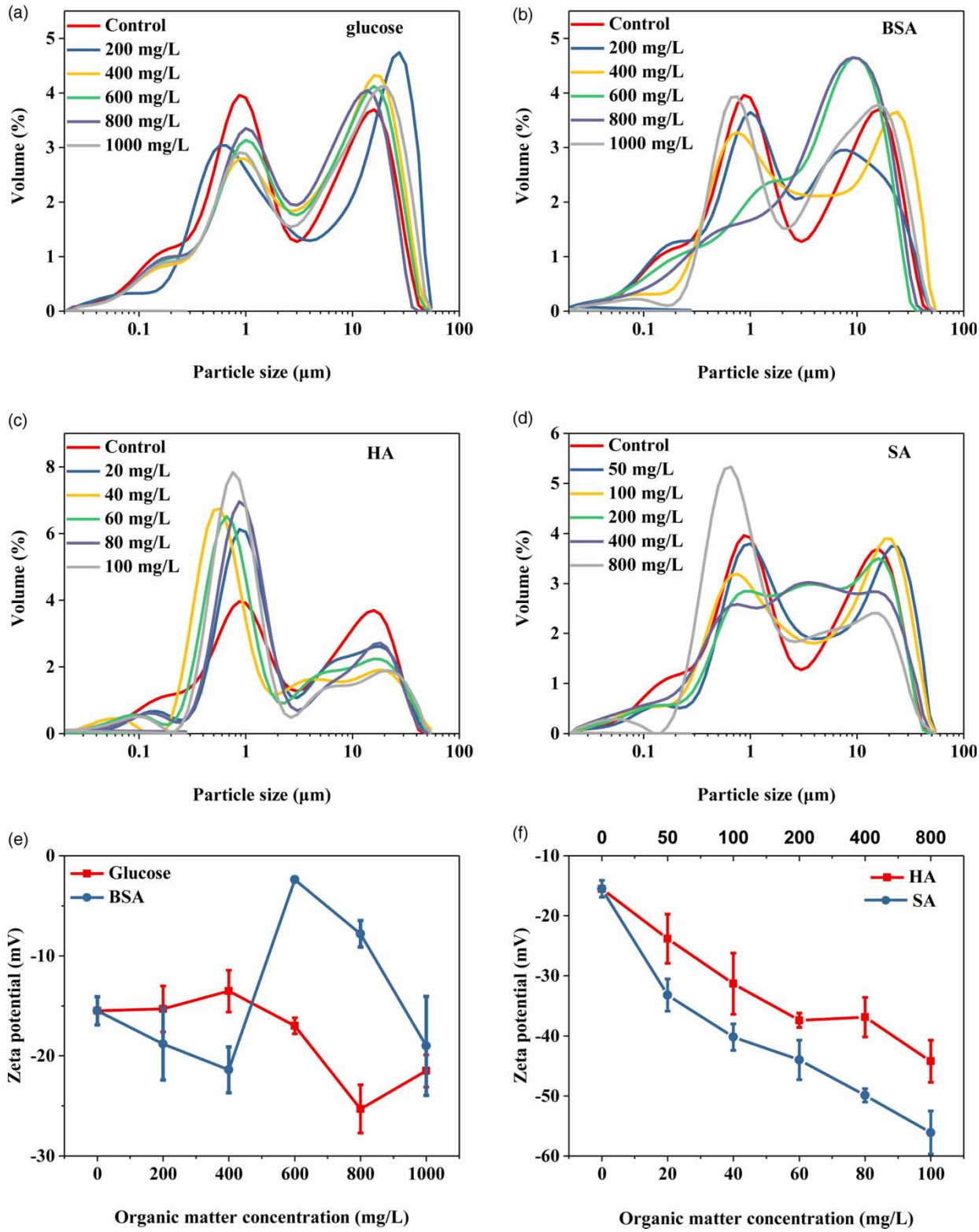

Figure 5 | The particle size and zeta potential of recovery products at different OM concentrations.

Mechanisms of different OM affecting the vivianite formation

The inhibition of P_R by OM was mainly caused by OM competing with PO_4^{3-} for Fe^{2+}. This was examined by increasing the molar Fe/P ratio in synthetic wastewater. In the presence of OM, Fe^{2+} was consumed by OM and became a limiting factor for P_R. The P_R was significantly improved (>97.0%) after Fe/P increased to 1.8, which supported the above deduction (Figure S4). In addition to competing for Fe^{2+}, OM might decrease the crystal growth rate through its adsorption on surface active growth sites of the crystals (Akin *et al.* 2008; Wei *et al.* 2017).

To validate the interaction of OM with vivianite, the precipitated products were analyzed by FTIR spectroscopy. As shown in Figure 6, without OM addition, the bands of products appeared at 3,480, 3,148, 1,622, 1,042, 970, 938, and 815 cm^{-1}. These absorption bands were consistent with vivianite crystals in the Sadtler standard spectra (Frost *et al.* 2002). Specifically, the broad peak between 3,480 and 3,148 cm^{-1} was attributed to the stretching vibration of hydroxyl groups. The band at 1,622 cm^{-1} was assigned to the bending mode of water hydrogen bonded to water. Three bands at 1,042, 970 and 938 cm^{-1} were attributed to the PO-stretching region. The band observed at 815 cm^{-1} was assigned to the water vibrational modes of strongly hydrogen bonded water molecules (Frost *et al.* 2002). In the presence of glucose and HA, no new absorption peaks were observed for the product (Figure 6). Bands of HA at 1,385 and 1,577 cm^{-1} were assigned to the asymmetric and symmetric carboxylate stretch (Wei *et al.* 2019). However, regardless of the dosage of HA, no bands of product at 1,385 and 1,577 cm^{-1} were detected, indicating that HA was not directly involved in vivianite formation. The

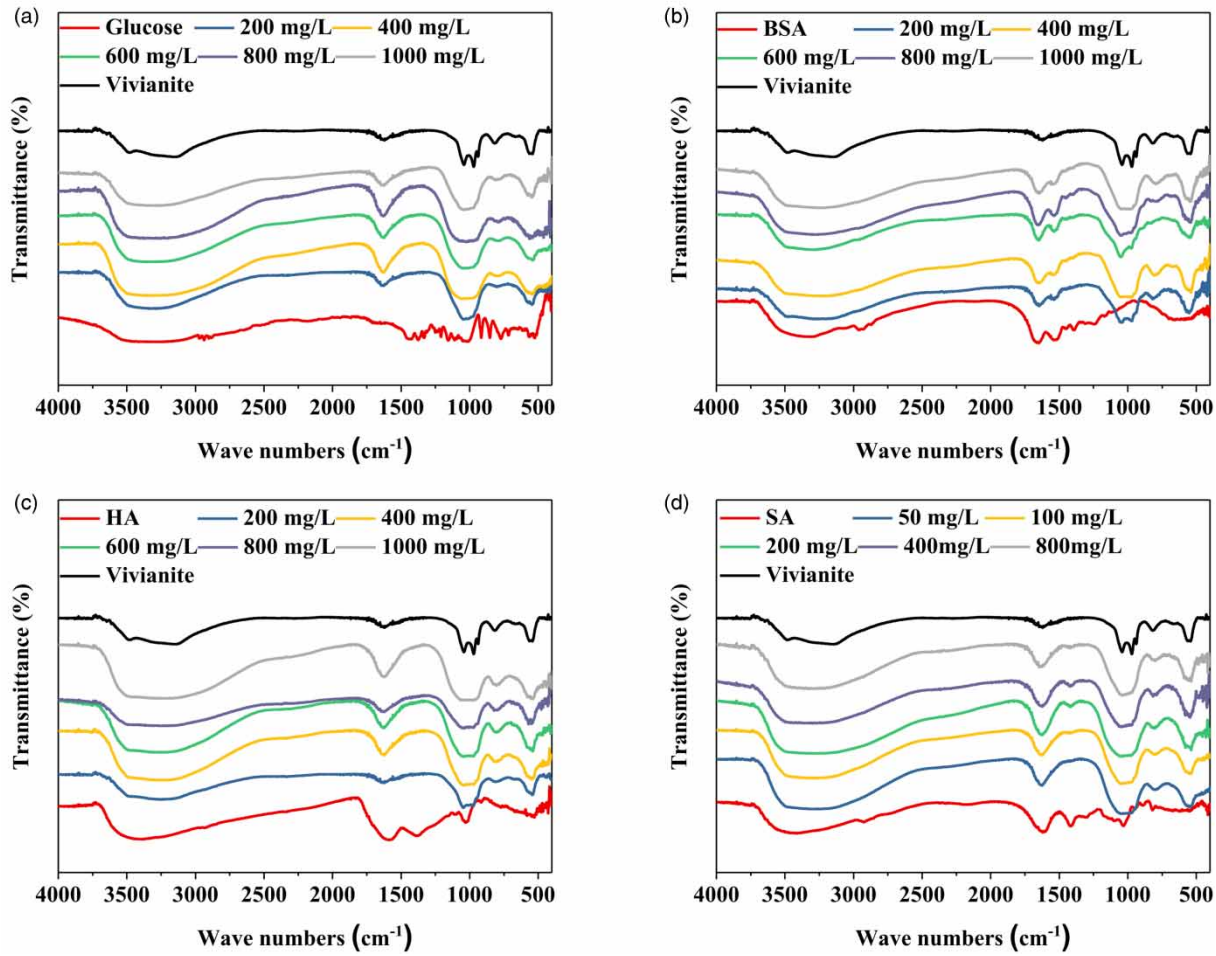

Figure 6 | FTIR spectra of recovered products under different OM: (a) glucose, (b) BSA, (c) HA and (d) SA.

interaction between HA and vivianite was weakly physical coprecipitation. In contrast with HA, the products with both BSA and SA addition exhibited new absorption bands. For BSA, the band located at 1,646 cm^{-1} came from C = O stretching and was attributed to the amide group of BSA (Liu *et al.* 2017). For SA, the bands that appeared at 1,416 and 1,543 cm^{-1} were assigned to the symmetric and asymmetric stretching vibrations of carboxyl groups (Cao *et al.* 2019). These results indicated that Fe^{2+} initially forms a binary complex with BSA or SA and then forms an insoluble vivianite-BSA or vivianite-SA complex.

Does this complexation affect the crystallization rate? According to Equation (3), *SI* was determined by the ionic activity of Fe^{2+} and PO_4^{3-}. The initial *SI* with different OM additions was the same before crystallization, so the difference in *SI* after the reaction can be used to evaluate the effect of OM on the crystallization rate. Based on Visual MINTEQ calculations, after crystallization, the *SI* with different OM are shown in Table S2. After reaction, the *SI* of the control, 1,000 mg/L glucose, 1,000 mg/L BSA, 100 mg/L HA and 800 mg/L SA were 5.85, 5.84, 6.46, 6.19 and 6.11, respectively. Compared with the initial *SI* (15.1), the *SI* after the reaction experienced rapid declines at different OM concentrations. It was indicated that crystallization rates were not significantly different. Therefore, the potential OM absorption on the vivianite active site was not the main reason for P_R reduction.

Based on the above discussion, a schematic diagram of OM reaction pathways during vivianite crystallization is illustrated in the graphical abstract. There was no inhibitory effect on the formation, morphology and structure of vivianite precipitates after glucose addition. BSA could combine with Fe^{2+}, but this part of Fe^{2+} could still react with PO_4^{3-} to form vivianite. Therefore, the presence of BSA could serve as a template and regulate the morphology of the crystals. This process is similar to biomimetic synthesis, which simulates the biomineralization process (Liu *et al.* 2017). The amide groups in BSA could enrich Fe^{2+} and provide nucleation sites. Then, the enriched Fe^{2+} would attract PO_4^{3-}, resulting in local supersaturation and increasing the growth rate. HA could bind with Fe^{2+} and inactivate it. Moreover, HA could coprecipitate on the vivianite surface and reduce the surface zeta potential, which would impede crystal aggregation growth. The mechanism of SA was similar to that of BSA, namely, it would precipitate during vivianite formation by direct physical precipitation and indirect chemical coprecipitation. In addition, SA would increase the solution viscosity and inhibit the aggregation growth and sedimentation of products.

Implications

Recently, P_R as vivianite from anaerobic fermentation supernatant has received more attention. However, OM in the supernatant would limit chemical P_R by vivianite crystallization. With vivianite precipitated from wastewater, the following process would take place:

$$3Fe^{2+} + xHPO_4^{2-} + yH_2PO_4^{-} + 8H_2O \rightarrow Fe_3(PO_4)_2 \cdot 8H_2O + zH^{+} \ (x + 2y = z). \quad (5)$$

The consumption of HPO_4^{2-} and $H_2PO_4^{-}$ resulted in a change in pH. The decrease in pH and the consumption of Fe^{2+} might cause a lower descent rate of *SI*. The ionic activity mainly depends on ionic strength of the solution. According to Visual MINTEQ calculations, at the same concentration of Fe^{2+} and PO_4^{3-}-P, a lower pH resulted in a smaller *SI*. To ensure a high recovery rate, keeping a stable reaction pH and raising the Fe/P ratio appropriately to obtain a higher *SI* may be a feasible approach. However, it is worth noting that with the decrease in *SI*, the rate of crystal formation also decreased. Therefore, to harvest vivianite efficiently within a limited crystallization time (100 min), the P concentration should be maintained at an optimum range (>5.0 mg/L).

The MW of organic substances is much larger than that of inorganic ions. The MW distribution of different OM is shown in Figure S5. It was found that OM with a lower MW weakly inhibited P_R. Thus, another feasible approach to enhance P_R is selectively removing high MW substances (HA and SA). From the perspective of morphology, reducing the concentration of HA and SA in wastewater helps to harvest larger vivianite crystals, which facilitates further separation.

CONCLUSION

Glucose, BSA, HA and SA were used to evaluate the effect of OM on vivianite crystallization. The results showed that glucose had no effect on P_R and vivianite morphology; BSA changed the vivianite morphology; HA reduced the P_R efficiency; and SA reduced the P_R efficiency with morphological changes. Mechanistic exploration indicated that Fe^{2+} inactivation by OM adsorption caused a reduction in P_R efficiency. The coprecipitation of HA on the vivianite surface decreased the vivianite particle size. The BSA and SA involved in vivianite internal provided nucleation sites and regulated vivianite aggregate morphology.

ACKNOWLEDGEMENTS

This work was supported by the Strategic Priority Research Program of the Chinese Academy of Sciences (CAS) (Grant No. XDA23,050,203). Additional support was provided by the Regional Key Project of STS of CAS (Grant No. KFJ-STS-QYZX-057), the Key Project of Shandong Provincial Natural Science Foundation (Grant No. ZR2020KE048) and the Key Research and Development Program of Shandong Province (Grant No. 2019GSF109002).

DATA AVAILABILITY STATEMENT

All relevant data are included in the paper or its Supplementary Information.

REFERENCES

Akin, B., Oner, M., Bayram, Y. & Demadis, K. D. 2008 Effects of carboxylate-modified, 'green' inulin biopolymers on the crystal growth of calcium oxalate. *Crystal Growth and Design* **8**, 1997–2005.

APHA 2005 *Standard Methods for the Examination of Water and Wastewater*. American Public Health Association, Washington, DC.

Cao, J., Wu, Y., Zhao, J., Jin, S., Aleem, M., Zhang, Q., Fang, F., Xue, Z. & Luo, J. 2019 Phosphorus recovery as vivianite from waste activated sludge via optimizing iron source and pH value during anaerobic fermentation. *Bioresource Technology* **293**, 122088.

Chen, Y., Jiang, S., Yuan, H., Zhou, Q. & Gu, G. 2007 Hydrolysis and acidification of waste activated sludge at different pHs. *Water Research* **41**, 683–689.

Chen, W., Teng, C., Qian, C. & Yu, H. 2019 Characterizing properties and environmental behaviors of dissolved organic matter using two-dimensional correlation spectroscopic analysis. *Environmental Science and Technology* **53**, 4683–4694.

Cheng, X., Chen, B., Cui, Y., Sun, D. & Wang, X. 2015 Iron(III) reduction-induced phosphate precipitation during anaerobic digestion of waste activated sludge. *Separation and Purification Technology* **143**, 6–11.

Chowdhury, R. B., Moore, G. A., Weatherley, A. J. & Arora, M. 2017 Key sustainability challenges for the global phosphorus resource, their implications for global food security, and options for mitigation. *Journal of Cleaner Production* **140**, 945–963.

Cordell, D., Drangert, J. & White, S. 2009 The story of phosphorus: global food security and food for thought. *Global Environmental Change* **19**, 292–305.

Desmidt, E., Ghyselbrecht, K. & Zhang, Y. 2015 Global phosphorus scarcity and full-scale P-recovery techniques: a review. *Critical Reviews in Environmental Science and Technology* **45**, 336–384.

Frost, R., Martens, W., Williams, P. & Kloprogge, J. 2002 Raman and infrared spectroscopic study of the vivianite-group phosphates vivianite, baricite and bobierrite. *Mineralogical Magazine* **66**, 1063–1073.

Garcia, C., Rieck, T., Lynne, B., Gali, A., Rougé, P. & Fàbregras, C. 2012 Struvite recovery: pilot-scale results and economic assessment of different scenarios. In: *Proceedings of IWA World Water Congress and Exhibition*. Busan, Korea.

Hao, X., Wang, C., Van Loosdrecht, M. C. M. & Hu, Y. 2013 Looking beyond struvite for P recovery. *Environmental Science and Technology* **47**, 4965–4966.

He, X., Xi, B. & Zhang, Z. 2014 Insight into the evolution, redox, and metal binding properties of dissolved organic matter from municipal solid wastes using two-dimensional correlation spectroscopy. *Chemosphere* **117**, 701–707.

Huang, W., Huang, W., Li, H., Lei, Z., Zhang, Z., Tay, J. & Lee, D. 2015 Species and distribution of inorganic and organic phosphorus in enhanced phosphorus removal aerobic granular sludge. *Bioresource Technology* **193**, 549–552.

Li, R. & Li, X. 2017 Recovery of phosphorus and volatile fatty acids from wastewater and food waste with an iron-flocculation sequencing batch reactor and acidogenic co-fermentation. *Bioresource Technology* **245**, 615–624.

Li, C. & Sheng, Y. 2020 Aqueous phosphate removal and electricity production using an iron-air fuel cell. *Journal of Environmental Engineering* **146**, 04020042.

Li, C., Sheng, Y. & Xu, H. 2020 Phosphorus recovery from sludge by pH enhanced anaerobic fermentation and vivianite crystallization. *Journal of Environmental Chemical Engineering*. doi:10.1016/j.jece.2020.104663.

Lin, Y., Sharma, P. & Van Loosdrecht, M. C. M. 2013 The chemical and mechanical differences between alginate-like exopolysaccharides isolated from aerobic flocculent sludge and aerobic granular sludge. *Water Research* **47**, 57–65.

Lin, H., Chen, Y., Shen, N., Deng, Y., Yan, W., Ruhyadi, R. & Wang, G. 2020 Effects of individual volatile fatty acids (VFAs) on phosphorus recovery by magnesium ammonium phosphate. *Environmental Pollution* **261**, 114212.

Liu, L., Wan, Y., Xie, Y., Zhai, R., Zhang, B. & Liu, J. 2012 The removal of dye from aqueous solution using alginate-halloysite nanotube beads. *Chemical Engineering Journal* **187**, 210–216.

Liu, Y., Chen, Y., Huang, X. & Wu, G. 2017 Biomimetic synthesis of calcium carbonate with different morphologies and polymorphs in the presence of bovine serum albumin and soluble starch. *Materials Science and Engineering C-Materials for Biological Applications* **79**, 457–464.

Liu, J., Cheng, X., Qi, X., Li, N., Tian, J., Qiu, B., Xu, K. & Qu, D. 2018 Recovery of phosphate from aqueous solutions via vivianite crystallization: thermodynamics and influence of pH. *Chemical Engineering Journal* **349**, 37–46.

Madsen, H. E. L. 2019 Influence of calcium and aluminum on precipitation of vivianite, $Fe_3(PO_4)_2{\cdot}8H_2O$. *Journal of Crystal Growth* **526**, 125242.

Park, S. & Yoon, T. 2009 Effects of iron species and inert minerals on coagulation and direct filtration for humic acid removal. *Desalination* **239**, 146–158.

Park, T., Ampunan, V., Maeng, S. & Chung, E. 2017 Application of steel slag coated with sodium hydroxide to enhance precipitation-coagulation for phosphorus removal. *Chemosphere* **167**, 91–97.

Shaddel, S., Ucar, S., Andreassen, J. & Osterhus, S. 2019 Engineering of struvite crystals by regulating supersaturation-Correlation with phosphorus recovery, crystal morphology and process efficiency. *Journal of Environmental Chemical Engineering* **7**, 102918.

Venkiteshwaran, K., McNamara, P. J. & Mayer, B. K. 2018 Meta-analysis of non-reactive phosphorus in water, wastewater, and sludge, and strategies to convert it for enhanced phosphorus removal and recovery. *Science of the Total Environment* **644**, 661–674.

Wang, F., Richards, V., Shields, S. & Buhro, W. 2014 Kinetics and mechanisms of aggregative nanocrystal growth. *Chemistry of Materials* **26**, 5–21.

Wang, Y., Xiao, Q., Zhong, H., Zheng, X. & Wei, Y. 2016 Effect of organic matter on phosphorus recovery from sewage sludge subjected to microwave hybrid pretreatment. *Journal of Environmental Science* **39**, 29–36.

Wang, S., An, J., Wan, Y., Du, Q., Wang, X., Cheng, X. & Li, N. 2018 Phosphorus competition in bioinduced vivianite recovery from wastewater. *Environmental Science and Technology* **52**, 13863–13870.

Wang, R., Wilfert, P., Dugulan, L., Goubitz, K., Korving, L., Witkamp, G. & Van Loosdrecht, M. C. M. 2019 Fe(III) reduction and vivianite formation in activated sludge. *Separation and Purification Technology* **220**, 126–135.

Wei, L., Hong, T., Liu, H. & Chen, T. 2017 The effect of sodium alginate on struvite crystallization in aqueous solution: a kinetics study. *Journal of Crystal Growth* **473**, 60–65.

Wei, L., Hong, T., Cui, K., Chen, T., Zhou, Y., Zhao, Y., Yin, Y., Wang, J. & Zhang, Q. 2019 Probing the effect of humic acid on the nucleation and growth kinetics of struvite by constant composition technique. *Chemical Engineering Journal* **378**, 122130.

Wilfert, P., Mandalidis, A., Dugulan, A., Goubitz, K., Korving, L., Temmink, H., Witkamp, G. & Van Loosdrecht, M. C. M. 2016 Vivianite as an important iron phosphate precipitate in sewage treatment plants. *Water Research* **104**, 449–460.

Wilfert, P., Dugulan, A., Goubitz, K., Korving, L., Witkamp, G. & Van Loosdrecht, M. C. M. 2018 Vivianite as the main phosphate mineral in digested sewage sludge and its role for phosphate recovery. *Water Research* **144**, 312–321.

Wu, Y., Luo, J., Zhang, Q., Aleem, M., Fang, F., Xue, Z. & Cao, J. 2019 Potentials and challenges of phosphorus recovery as vivianite from wastewater: a review. *Chemosphere* **226**, 246–258.

Yang, X., Du, M., Lee, D., Wan, C., Zheng, L. & Wan, F. 2012 Improved volatile fatty acids production from proteins of sewage sludge with anthraquinone-2,6-disulfonate (AQDS) under anaerobic condition. *Bioresource Technology* **103**, 494–497.

Yuan, Z., Pratt, S. & Batstone, D. 2012 Phosphorus recovery from wastewater through microbial processes. *Current Opinion in Biotechnology* **23**, 878–883.

Yuan, R., Shen, Y., Zhu, N., Yin, C., Yuan, H. & Dai, X. 2019 Pretreatment-promoted sludge fermentation liquor improves biological nitrogen removal: molecular insight into the role of dissolved organic matter. *Bioresource Technology* **293**, 122082.

Zelibor, J. L., Senftle, F. E. & Reinhardt, J. L. 1988 A proposed mechanism for the formation of spherical vivianite crystal aggregates in sediments. *Sedimentary Geology* **59**, 125–142.

Zhang, C., Hu, D., Yang, R. & Liu, Z. 2020 Effect of sodium alginate on phosphorus recovery by vivianite precipitation. *Journal of Environmental Science* **93**, 164–169.

Zhou, Z., Hu, D., Ren, W., Zhao, Y., Jiang, L. & Wang, L. 2015 Effect of humic substances on phosphorus removal by struvite precipitation. *Chemosphere* **141**, 94–99.

First received 4 January 2021; accepted in revised form 15 March 2021. Available online 23 March 2021